J Mater Sci: Mater Med (2011) 22:437–450
DOI 10.1007/s10856-010-4224-0

# Effect of the environment on wear ranking and corrosion of biomedical CoCrMo alloys

**A. Igual Muñoz · S. Mischler**

Received: 30 June 2010 / Accepted: 21 December 2010 / Published online: 11 January 2011


**Abstract** The corrosion behaviour and the wear ranking of biomedical high carbon (HC) and low carbon (LC) CoCrMo alloys sliding against an alumina ball in four different simulated body fluids [NaCl and phosphate buffered solutions (PBS) with and without albumin] has been analyzed by tribocorrosion and electrochemical techniques. The effects of alloy and of albumin on corrosion depend on the base electrolyte: differences between LC and HC alloy were only observed in NaCl solutions but not in PBS. Albumin increased significantly corrosion of both alloys in PBS solutions while its effect in NaCl was smaller. The wear ranking of the HC and LC alloys also depends on the environment. In the present study, HC CoCrMo alloy had lower wear resistance in NaCl and PBS + albumin than the LC alloy, while no differences between both alloys were found in the other solutions. This was attributed to surface chemical effects affecting third body behaviour.

## 1 Introduction

Cobalt chromium molybdenum alloys are widely used in orthopaedic implants due to their high mechanical resistance combined with good corrosion properties in body fluids. The latter are due to the formation of a passive film mainly composed by chromium oxide. Their favourable tribological behaviour make these alloys particularly suitable for metal on metal bearing surface for artificial joint implants [1]. However, concern exists about the long-term stability of such bearing surfaces. In fact, despite the low wear and corrosion rates, accumulation of wear particles and dissolved ions in the body are known to cause adverse clinical responses affecting the stability of the implant [2, 3]. Therefore, several studies were devoted to identify the mechanisms and the critical factors affecting material release in order to develop more wear resistant CoCrMo implant alloys. Among these, design parameters such as clearance and material type have been identified as affecting wear and clinical lifetime of metal on metal implants [1].

The mechanisms governing material release are quite complex as they imply the interaction of mechanical parameters (contact pressure, sliding velocity, lubrication), surface chemical effects (metal oxidation and dissolution, adsorption of organic molecules present in the body fluids) and materials properties (composition, microstructure, hardness) that determine wear and corrosion. In such situations material degradation proceeds by the interaction of mechanical (wear) and surface chemical effects (corrosion) that is usually designated as tribocorrosion [4]. This complexity clearly poses problems for the in vitro ranking of implant materials as well as for the mechanistic interpretation of the results.

In the past years effort was done in order to identify whether high carbon (HC) (>0.15% weight) or low carbon (LC) content of CoCrMo alloys was more appropriate for artificial joints implants [4–17]. The main difference between the two alloys is the presence of chromium carbides in the HC alloys that increase hardness but affect the corrosion stability by depleting the metal matrix in

A. Igual Muñoz (✉)
Departamento de Ingeniería Química y Nuclear,
E.T.S.I. Industriales, Universitat Politècnica de València,
P.O. Box 22012, 46071 Valencia, Spain
e-mail: anigmu@iqn.upv.es

S. Mischler
Tribology and Interface Chemistry Group (Station 12,
SCI-STI-SM), Swiss Federal Institute of Technology Lausanne
(EPFL), 1015 Lausanne, Switzerland
e-mail: stefano.mischler@epfl.ch

chromium [18]. Despite the fact that no significant difference in wear between LC CoCrMo or HC CoCrMo was observed in retrieved artificial hip joints [1], in vitro investigations in general rather indicate that HC alloys are more wear resistant. Table 1 summarizes the conditions and the outcomes of the published in vitro studies comparing the wear behaviour of LC and HC alloys in simulated body fluids. It is evident that the studies listed in Table 1 were carried out under a diversity of conditions implying different wear test rigs, different materials and lubricants that do not necessarily reflect the entire in vivo situation. In this sense, in vitro tests need improvements in order to increase their reliability for material ranking.

Not surprisingly some discrepancies are observed in the results, in particular concerning the ranking of HC and LC alloys. Indeed, Yan et al. [4, 17], Wang et al. [6], Cawley et al. [12], Scholes et al. [9], observed higher wear in the LC alloy while St. John et al. [8] and Scholes et al. [9] observed no differences between the alloys. St John [11] found that the lowest wear rates were achieved in a LC/HC coupling.

Despite these discordancies, that probably reflect the complexity of the involved phenomena, those studies yielded interesting information concerning mechanisms and critical factors determining wear.

High concentration of carbides was found to enhance wear resistance by Cawley et al. [12]. On the other hand Chiba et al. [16] found that self mated carbide free alloys contacts are more resistant to fatigue wear and exhibit less abrasive wear than HC alloy contacts. Wang et al. [5] observed that initially standing proud carbides were worn below the metal surface or pulled out from the matrix causing potential risk of three body abrasive wear. Clearly the role of carbides is complex and depends on the

**Table 1** Papers published on the wear behaviour comparison between low carbon and high carbon CoCrMo alloys

| Ref. | Year | Alloys | Carbon content | Solution | Contact |
|---|---|---|---|---|---|
| [5] | 1999 | ASTMF1537-94 | C 0.05 | Serum | Hip simulator |
| | | | C 0.2 | | |
| [6] | 1999 | ASTMF1537 | C 0.04–0.05 | Serum + 0.2% sodium azide | Oscillating cylinder on concave plate |
| | | | C 0.2–0.25 | | |
| [7] | 1999 | ASTMF1537 | C 0.07 | Serum + 0.1% sodium azide | Ball (100 mm radius) on flat Metal-on-Metal |
| | | | C 0.2 | | Reciprocating + rotation |
| [8] | 1999 | ASTMF1537 | C 0.06 | Serum + 20 mM EDTA | Hip simulator |
| | | | C 0.24 | | |
| [9] | 2001 | ASTMF1537 | C 0.06 | Serum + 0.2% sodium azide | Pin on plate Metal-on-Metal |
| | | | C 0.25 | | Reciprocating + rotation |
| [10] | 2001 | ASTMF1537 | C <0.07 | Serum + 0.1% sodium azide | Hip simulator |
| | | | C >0.2 | | |
| [11] | 2003 | ASTMF1537-02 | C 0.05 | Serum + 20 mM EDTA | Pin on disc reciprocating |
| | | | C 0.24 | | |
| [12] | 2003 | ASTM F-75 98 | C 0.28 | Water | Microabrasion |
| | | As cast, HT, HIP, HIP + HT | | | Steel counterpiece |
| [13] | 2004 | ASTMF1537 | LC | Serum | Pin on plate reciprocating linear |
| | | Several HT | HC | | |
| [14] | 2006 | $Co_{27}Cr_6Mo$ | C 0.054 | Dry | Cylinder on flat Metal-on-Metal |
| | | $Co_{27}Cr_6Mo$ | C 0.197 | | 440 MPa average |
| [4] | 2006 | ASTMF1537-97 | C 0.051 | Serum + 20 mM EDTA | Reciprocating pin-on-plate |
| | | ASTMF75-97 | C 0.23 | | |
| | | | C 0.27 | | |
| [15] | 2006 | $Co_{27}Cr_6Mo$ | C 0.19 | Calf serum | SiN ball on flat |
| | | $Co_{27}Cr_6Mo$ | C 0.05 | DMEM | Reciprocating |
| | | | | NaCl | |
| [16] | 2007 | ASTM F-75 98 | Cast C 0.26 | Hanks | Pin on disk |
| | | Cast, forged | Forged C 0.067 | | Self mated |
| [17] | 2007 | $Co_{27}Cr_6Mo$ | C 0.19 | DMEM | SiN ball on flat |
| | | $Co_{27}Cr_6Mo$ | C 0.05 | NaCl | Reciprocating |

*HT* heat treated, *HIP*, hot isostatic pressure, *DMEM* Dulbecco's modified Eagle's medium

prevailing wear mechanism (abrasion, fatigue), on their wear resistance and cohesion to the matrix.

Varano et al. [14, 15] pointed out that carbon dissolved in the matrix governs the strain-induced transformation responsible for work hardening. In fact, dissolved carbon is supposed to stabilize the cubic face centred phase and thus inhibits the strain-induced transformation in the hexagonal close packed structure. Chiba et al. [16] observation that the strain induced transformation is inhibited in HC alloys lends support to this hypothesis. In an earlier work Varano et al. [13] observed that increasing amount of dissolved carbon lead to reduction in wear.

The nature of the antagonist is a crucial factor: St John et al. [11] and Firkins et al. [10] observed that self mated LC alloys contacts wear more than self mated HC alloy contacts. Interestingly both authors found that the wear behaviour of a contact involving LC and HC alloys is similar or even better than self mated HC alloy contacts.

Kinematics also affects the ranking of LC and HC alloys. Scholes et al. [9] observed significantly higher wear of a LC alloys subject to reciprocating sliding wear compared to a HC alloy. However superimposing a rotation to sliding suppressed differences between the two alloys and reduced wear. This latter effect was also reported by Tipper et al. [7] who moreover pointed out the relevance for wear of boundary and fluid film lubrication as well as of third bodies.

Surprisingly, the effect of environment chemistry on LC/HC ranking was not considered despite the fact that the test solution was found to profoundly affect the wear behaviour of CoCrMo alloys in simulated body fluids [4]. Other in vitro [4, 19–22] and retrieval [23] studies of CoCrMo implants found that the governing wear mechanisms are predominantly tribocorrosion reactions involving the interaction of bio- and surface-chemical (corrosion) and mechanical (wear). Thus the wear behaviour is expected to change depending on environment chemistry. This is a particularly relevant point for pre-clinical evaluation of artificial joints through tests carried out in simulated body fluids of varying concentration and chemical composition (diluted calf serum, Dulbecco's Modified Eagle's Medium, Hank's, Ringer or PBS solutions) that hardly reflects the in vivo chemistry of synovial fluids.

The aim of this paper is to evaluate the influence of solution chemistry on the wear ranking of a LC and a HC CoCrMo biomedical alloy. For this tribocorrosion tests were carried out using a reciprocating ball (alumina) on plate (CoCrMo alloy) contact configuration immersed in different simulated body fluids [NaCl and phosphate buffered solutions (PBS) with or without addition of albumin as model protein]. The tests were carried out under controlled electrochemical conditions allowing for quantification of metal oxidation during sliding. The pure corrosion behaviour was characterised by measuring polarisation curves.

## 2 Materials and methods

### 2.1 Solutions and materials

The electrolytes employed consisted of 0.14 M NaCl solution and simulated body fluid which was prepared with the following composition: 0.14 M NaCl, 1 mM $KH_2PO_4$, 3 mM KCl, 10 mM $Na_2HPO_4$ (a PBS, pH 7.4). In order to analyze the protein effect on the corrosion behaviour of the materials, the same solutions were prepared with 0.5 g/l albumin. The non-buffered solutions were adjusted to pH 7.4 with the addition of concentrated HCl or concentrated NaOH before each experiment. The temperature of the solution was maintained at 37°C, unless otherwise stated.

Samples were extracted by spark erosion from hip joint simulator heads made out of HC or LC ASTM F 1537-00 CoCrMo alloys (heads supplied by PlusOrthopedics, Aarau). A surface area of 0.28 $cm^2$ was exposed to the test solution during experiments. The alloys composition was determined by X-ray fluorescence and is given in Table 2. According to the ASTM F 1537-00 standard, the carbon content of the LC alloy ranges from 0 to 0.14% w while the HC alloy contains from 0.15 to 0.35 w% carbon. Etching using a permanganate solution (100 ml water + 4 g $KMnO_4$ + 4 g NaOH) was used to reveal the carbide grains. The HC alloy contains dispersed carbides with grain sizes ranging from typically 0.4 to 3.3 μm. No carbides could be observed on the LC alloy.

### 2.2 Electrochemical tests

Potentiodynamic curves were measured using an Autolab PSTAT 30 potentiostat. The cell was a three-electrode cell, with platinum wire counter electrode and a standard calomel reference electrode (SCE). All potentials in this paper are given with respect to this reference electrode. The samples were ground with SiC emery paper up to 1,000 grit before each experiment. After cleaning and rinsing with

**Table 2** Chemical composition in wt% of the investigated alloys (X-ray fluorescence analysis)

| Element | HC alloy | LC alloy |
|---|---|---|
| Fe | 0.35 | 0.24 |
| Co | 63.67 | 64.95 |
| Cr | 29.68 | 28.80 |
| Mo | 5.69 | 5.68 |
| Ni | 0.58 | 0.32 |

water and ethanol the polished sample was instantly assembled into the measurement cell and subsequently the electrolyte was filled in the cell. Before potentiodynamic measurements, the electrode was left stabilising at open circuit potential for 20 min. Afterwards, the potential was swept with a sweep rate of 2 mV $s^{-1}$, starting at −1500 mV and ending at 1500 mV. All experiments were carried out under aerated conditions.

### 2.3 Tribocorrosion tests

The investigated tribosystem involved a contact between a stationary CoCrMo disk (20 mm in diameter, thickness 3 mm) and a moving alumina ball of 6 mm diameter supplied by SWIP AG Brugg with a surface finish of 0.02 μm $R_a$ (according to the manufacturer). All experiments were carried out on an alternating motion tribometer, described in previous studies [24–26]. The tribometer operated with an integrated electrochemical cell (three-electrode cell) including the specimen as working electrode, a Pt wire counter electrode and a Calomel reference electrode. The same solutions described in the electrochemical tests were used for the tribocorrosion assays. The linear motor (ETEL SA Môtiers) providing motion was driven by a truncated triangular wave signal resulting in a ball oscillation frequency of 1 Hz and a stroke length of 5 mm. The ball was maintained motionless for 25 ms at the end of each stroke. A normal load of about 1.2 N was applied. The electrochemical cell was fixed on a load cell, allowing for the measurement of the applied normal force. The frictional force was measured by means of a piezoelectric force transducer. During the experiments, the frictional and the normal forces, the vertical and horizontal pin displacement as well as the electrochemical parameters, namely current and potential, were monitored using a Macintosh computer running under Labview software. Each parameter was acquired at a sampling rate of 1,000 points per second and, simultaneously, the mean value was calculated every second. The mean frictional coefficient was calculated by dividing the tangential force by the normal force when the ball was in the middle of the stroke. All tests were repeated twice to check for reproducibility.

The samples were ground with SiC emery paper up to 4,000 grit and polished with diamond paste until reaching a mirror-like surface finishing before each experiment (<0.1 μm Ra). Before the tests, the samples were cleaned in an ultrasonic acetone bath for 3 min, rinsed with ethanol, then cleaned in an ultrasonic ethanol (for analysis) bath for 3 min, rinsed with doubly distilled water and dried in a stream of $N_2$. The alumina balls were cleaned before the test in an ultrasonic ethanol (p.a.) bath for 3 min and rinsed with doubly distilled water. After mounting the specimen and the counterpart on the tribometer, the selected solution was poured into the electrochemical cell and the temperature was set and maintained at 37 ± 1°C. The counterpart motion was provided by a linear motor. The test procedure was carried out using the following steps:

- Immersion of the CoCrMo disk in the electrolyte under open circuit conditions (OCP) during 2 min.
- Cathodic polarization at −1.2 V/SCE during 5 min.
- Return to OCP conditions, measurement of the corrosion potential during 5 min.
- Polarization at −0.1 V/SCE for 15 min.
- Sliding during 1 h while the polarization is maintained.
- Sliding is stopped, the polarization is maintained for 5 min.

Wear was quantified using a non contact laser scanning profilometer UBM instrument. For this, three profiles were measured across the wear track for each sample. The wear track volume was determined by multiplying the area of the profiles situated at heights below 0 (reference level corresponded to the non rubbed area) and multiplying it by the length of the wear track. Optical microscope and a scanning electron microscope, SEM, (JEOL6300) were used to analyze wear tracks on the metal's disks and on the alumina counterparts.

## 3 Results

### 3.1 Polarisation curves

Typical polarization curves of the HC and LC alloys in NaCl and PBS solutions with and without albumin are shown in Fig. 1. To facilitate comparison, the following data were extracted form the polarisation curves and listed in Table 3: corrosion potential $E_{corr}$ (potential at which the current changes sign), the corrosion current density $i_{corr}$ (extracted through extrapolation of Tafel slopes at the corrosion potential), and the passive current density $i_p$ measured at a potential of −0.1 V.

Differences between both alloys are observed in NaCl solutions (Fig. 1a) where the HC CoCrMo alloy presents lower corrosion potential values and higher passive current densities. The LC alloy exhibits a shoulder at the end of the passive plateau at approximately 0.1 V. Albumin does not significantly modify the polarisation curve of the HC alloy while has some minor effects on the polarization behaviour of the LC alloy in the cathodic domain close to the corrosion potential and on the shoulder observed before the transpassive domain.

In the PBS solutions (Fig. 1b) differences in polarisation behaviour between the two alloys disappear. Only in the passive domain, the HC alloys exhibits slightly higher passive current densities as already observed in the NaCl

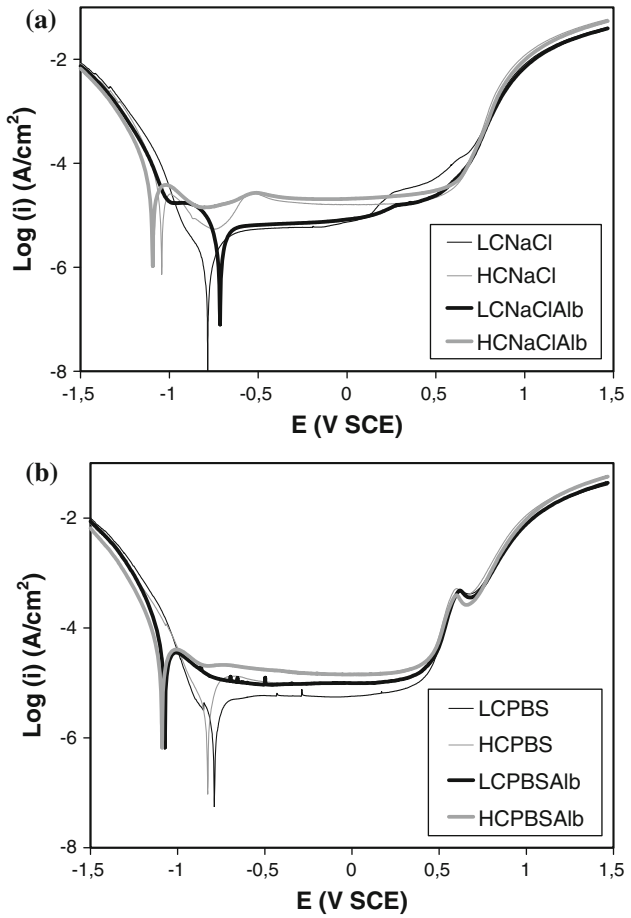


**Fig. 1** Potentiodynamic curves for HC and LC alloys in **a** 0.14 NaCl and **b** PBS with and without albumin (pH 7.4, 37°C)

solution. In the PBS solution and for both alloys, albumin shifts the corrosion potential towards more negative values and increases the current density in the passive domain.

## 3.2 Friction

The typical evolution of the friction coefficient and of the current during tribocorrosion experiments is illustrated Fig. 2. In general the coefficient of friction reaches rapidly an initial steady state value of approximately 0.4. In three cases (LC alloy in absence of albumin, HC alloy in PBS only) a transition to higher values (0.9–1) of friction is observed (Fig. 2a). The alloy type has no significant effect on friction while albumin significantly reduces friction in the PBS solutions. In the NaCl solution its lubricating effect depends on the alloy type: albumin has no effect on the HC alloy while it suppresses the transition to higher coefficient of friction in the case of the LC alloy. For comparison purpose, the values of the coefficient of friction averaged over the entire sliding period are listed in Table 4 for different experimental conditions.

## 3.3 Electrochemical response during sliding

Figure 2 shows that at the onset of the sliding the current increases sharply from 0.05 μA up to values between 0.015 and 0.02 mA. After stopping the sliding the current decreases again to the initial value observed before sliding. This behaviour is usually attributed to the repassivation of the bare metal exposed to the solution by deformation and wear of the passive alloys [27]. Large noise on the current signal is observed in the initial stages of the sliding except in presence of albumin. The transitions in coefficient of friction are accompanied by a noise reduction in current with no significant alteration of the average value (Fig. 2a). Both alloys exhibit in the NaCl + albumin solution (Fig. 2c, d) a transition from higher to lower current after a sliding time ranging from 400 to 1000 s approximately. Interestingly, these transitions in current do not correspond to changes in friction and do not occur in the PBS + albumin solution, at least within the test duration. The transition occurs earlier in the case of the LC alloy. Similar transitions in current were reported by Yan et al. [17] who also observed the earlier reaction of the LC alloy only in solutions containing organic molecules.

The average anodic current during sliding $I_{sliding}$ was calculated by subtracting from the current measured during sliding the value of the current measured before starting the

**Table 3** Results of the electrochemical parameters for HC and LC CoCrMo alloys in the studied solutions

| Alloy | NaCl | NaCl + albumin | PBS | PBS + albumin |
|---|---|---|---|---|
| $E_{cor}$ ($V_{SCE}$) | | | | |
| HC | −1.04 ± 0.02 | −1.09 ± 0.02 | −0.83 ± 0.005 | −1.09 ± 0.001 |
| LC | −0.79 ± 0.01 | −0.68 ± 0.02 | −0.79 ± 0.001 | −1.10 ± 0.001 |
| $i_{cor}$ (μA/cm$^2$) | | | | |
| HC | 9.3 ± 1.0 | 11.0 ± 0.5 | 2 ± 0.1 | 11.3 ± 0.1 |
| LC | 0.5 ± 0.1 | 1.5 ± 0.5 | 1.0 ± 0.1 | 11.4 ± 0.1 |
| $i_p$ (μA/cm$^2$) | | | | |
| HC | 16.1 ± 0.5 | 20.7 ± 0.5 | 9.9 ± 0.2 | 14.2 ± 0.2 |
| LC | 5.8 ± 0.5 | 7.2 ± 0.5 | 5.7 ± 0.2 | 9.9 ± 0.2 |

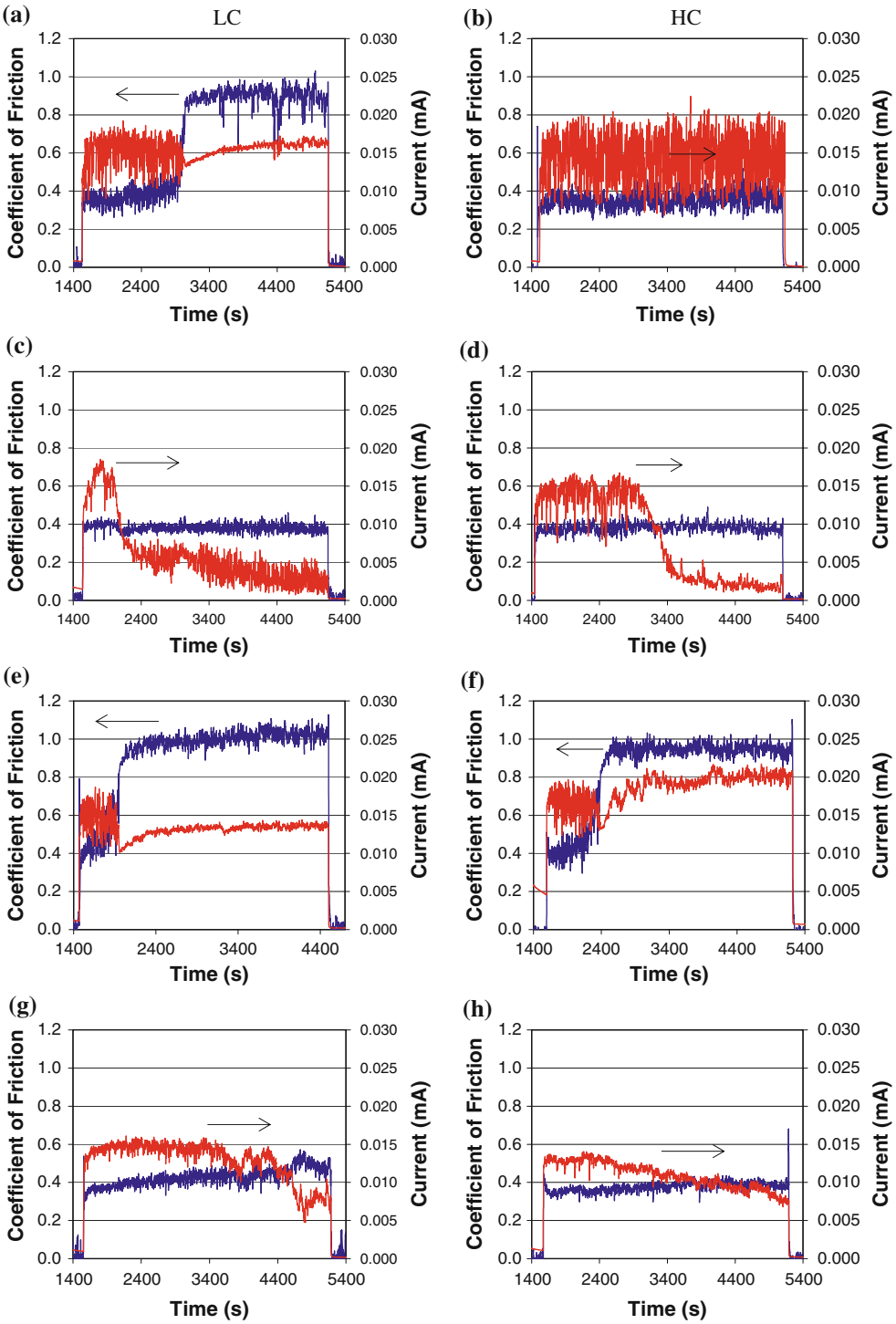


**Fig. 2** Evolution of the mean coefficient of friction and current of LC and HC during sliding in **a**, **b** NaCl; **c**, **d** NaCl + albumin; **e**, **f** PBS and **g**, **h** PBS + albumin. Normal load is 1.2 N and applied potential −0.1 $V_{SCE}$

sliding. Obtained values are listed in Table 4. The average values of the anodic current of both alloys decreases in PBS when compared to the current values measured in NaCl solution. Albumin has a major effect on the current at the end of the sliding. Its effect consists on diminishing the average values to those close to the passive values observed before the sliding. Albumin also decreases the current values during sliding of HC and LC in the NaCl solutions. PBS hinders this albumin effect in both alloys.

### 3.4 Wear

Figure 3 shows typical wear track cross sections measured by profilometry on HC and LC alloys in albumin

**Table 4** Effect of solution chemistry and CoCrMo alloy on the wear volume, coefficient of friction, current during sliding and transition time in friction and current

| | Wear volume ($10^{-3}$ mm$^3$) | Friction | Current (mA) × $10^{-3}$ | Transition time in friction (s) | Transition time in current (s) |
|---|---|---|---|---|---|
| HC | | | | | |
| NaCl | 2.27 | 0.36 | 15.7 | +3600 | |
| | 2.43 | 0.37 | 13.6 | | |
| | 2.3 | 0.48 | 12.8 | | |
| NaCl + albumin | 1.20 | 0.38 | 7.3 | | 1116 |
| | 1.12 | 0.38 | 5.2 | | 1682 |
| | 1.15 | 0.32 | 5.3 | | 1124 |
| PBS | 1.40 | 0.85 | 9.7 | 640 | |
| | 1.39 | 0.82 | 12.8 | 1170 | |
| | 1.40 | 0.72 | 10.5 | 692 | |
| PBS + albumin | 1.90 | 0.40 | 10.4 | | |
| | 1.90 | 0.38 | 9.2 | | |
| | 1.87 | 0.40 | 8.1 | | |
| LC | | | | | |
| NaCl | 1.85 | 0.69 | 14.6 | 1328 | |
| | 2.00 | 0.62 | 14.6 | 1710 | |
| | 1.90 | 0.65 | 14.4 | 1500 | |
| NaCl + albumin | 1.36 | 0.35 | 4.0 | | 1804 |
| | 1.10 | 0.38 | 2.4 | | 494 |
| | 1.19 | 0.40 | 3.9 | | 392 |
| PBS | 1.36 | 0.89 | 10.5 | 420 | |
| | 1.26 | 0.84 | 9.6 | 430 | |
| | 1.30 | 0.91 | 10.2 | 340 | |
| PBS + albumin | 0.78 | 0.43 | 5.2 | | |
| | 1.40 | 0.42 | 11.0 | | |
| | 1.40 | 0.45 | 11.2 | | |

Normal load is 1.2 N and applied potential −0.1 $V_{SCE}$

containing solutions. The wear volumes extracted from the cross sections are listed in Table 4.

Optical microscope images of the wear tracks are shown in Fig. 4 for the different experimental conditions. The wear tracks show a predominantly abrasive mechanism as evidenced by the presence of scratches over the entire scar length. A significant amount of relatively large (μm size) debris was found accumulating around the track in the NaCl solution for both alloys while less debris particles are visible in the PBS solution. The presence of albumin significantly reduces their quantity for both solutions and alloys.

SEM images representing the typical topography found in the center of the wear tracks are shown in Fig. 5. Worn surfaces of LC alloy are relatively smooth and, except some fine scratches observed in the NaCl + albumin solution (Fig. 5c), rather featureless. The HC alloy exhibits in absence of albumin marked micrometer wide scratches parallel to the sliding direction (Fig. 5b, f). In presence of albumin these large scratches are no longer observed and in the NaCl solution the wear track of the HC alloy is as smooth as in the case of the LC alloy (Fig. 5d) while in PBS scratches are dominant.

Isolated debris particles are observed on all worn surfaces although their size and number varies with solution composition and alloy (Fig. 6). In the NaCl + albumin solution the debris particles observed on both alloys are elongated and appears to be formed by agglomeration in rolls of very fine nanometer sized particles (Fig. 6b). In the other conditions (Fig. 6a) the debris particles are larger and of isotropic dimensions. They appear to fragment in smaller, looser particles. The HC alloy exhibits a larger number of particles than the LC alloy in the NaCl or PBS solutions in absence of albumin.

The transitions in current and friction are associated with a change in wear and debris particles morphology. Figure 7 shows SEM images taken in the centre of wear tracks formed during experiments stopped before the

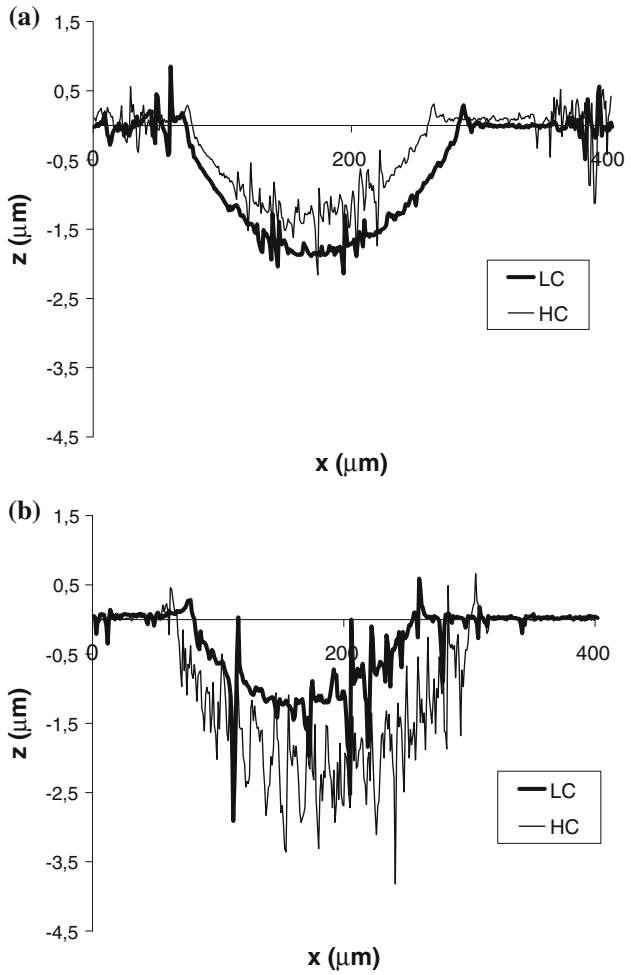


**Fig. 3** Wear profiles on two discs of HC and LC after tests in **a** NaCl with albumin and **b** PBS with albumin. Normal load is 1.2 N and applied potential −0.1 $V_{SCE}$

transitions in friction (Fig. 7a) and current (Fig. 7b) occur. Non-fragmented, round shaped debris particles are observed before transition in friction (Fig. 7a). After this transition, the particles are smaller and appear to fragment, as it was observed in Fig. 6a. With respect to the appearance of wear debris before the transition in current, large (micrometer size) particles formed by agglomeration of smaller entities are found. Beside this some smaller submicron sized round particles can be also observed, Fig. 7b. The typical roll like particles observed after wear test in albumin solution (Fig. 6b) are not found before this current transition. Clearly, the latter is associated to a change in particle morphology.

Alumina balls were examined by optical microscopy after the tribocorrosion test. No abrasion of the balls could be observed although the rubbed area was systematically found surrounded by transferred debris particles. Appearance of alumina balls after the tribocorrosion tests was similar among the different experimental conditions considered in this study. However, no quantification of the transferred material was carried out so that differences in the amount of transfer cannot be excluded.

## 4 Discussion

### 4.1 Polarization behaviour

The data from Table 3 clearly indicate that the LC alloys has significantly lower corrosion current densities in most of the solutions than the HC alloy. Only in the PBS + albumin solution the corrosion current densities were similar. The effect of solution is more complex. The PBS solution reduces the corrosion current density of the HC alloy while has an opposite effect on the LC alloy. Albumin increases the corrosion rate independently on alloy and solution. However, the most pronounced effect appears in the PBS solution for both alloys. These variations in current densities can be rationalized by considering the potential at which they were measured (corrosion potential). In Fig. 8 the current density values (Table 3) were plotted against the corrosion potential for all the tested alloys. This figure clearly shows that the current density increases with decreasing potentials and this independently on alloy and solution. Such behaviour was already reported in the literature [28]. Close to the corrosion potential a Tafel behaviour (logarithmic relationship between current and potential) was observed in all tested conditions. This suggests that the metal is in an active state where the kinetics are controlled by the charge transfer at the metal/solution interface [29]. In this case, according to the mix potential theory of corrosion, the observed trend in corrosion current with potential can be only explained by an increase of the anodic reaction rate. Indeed anodic dissolution can be influenced by several factors such as metal composition and microstructure as well as adsorption of organic and inorganic species.

The variations in corrosion current depending on experimental condition can be, at least in a first approximation, explained by this effect. In NaCl and NaCl + albumin the dissolution rate seems to be mainly controlled by the alloy composition. Indeed in the HC alloy a significant part of Cr is bound in $Cr_{21}Mo_2C_6$ carbides [30] and thus the chromium depleted metal matrix is expected to be more prone to corrosion than the LC alloy. This is indeed evidenced in Table 3.

In PBS solutions the role of solution chemistry becomes more pronounced and hides the alloy effect. Phosphate ions are known to adsorb on CoCrMo surfaces and thus to act as anodic inhibitors [18, 31]. The inhibition effect is effectively observed with the HC alloy but not with the LC alloy where the dissolution rate is already low. Albumin has a

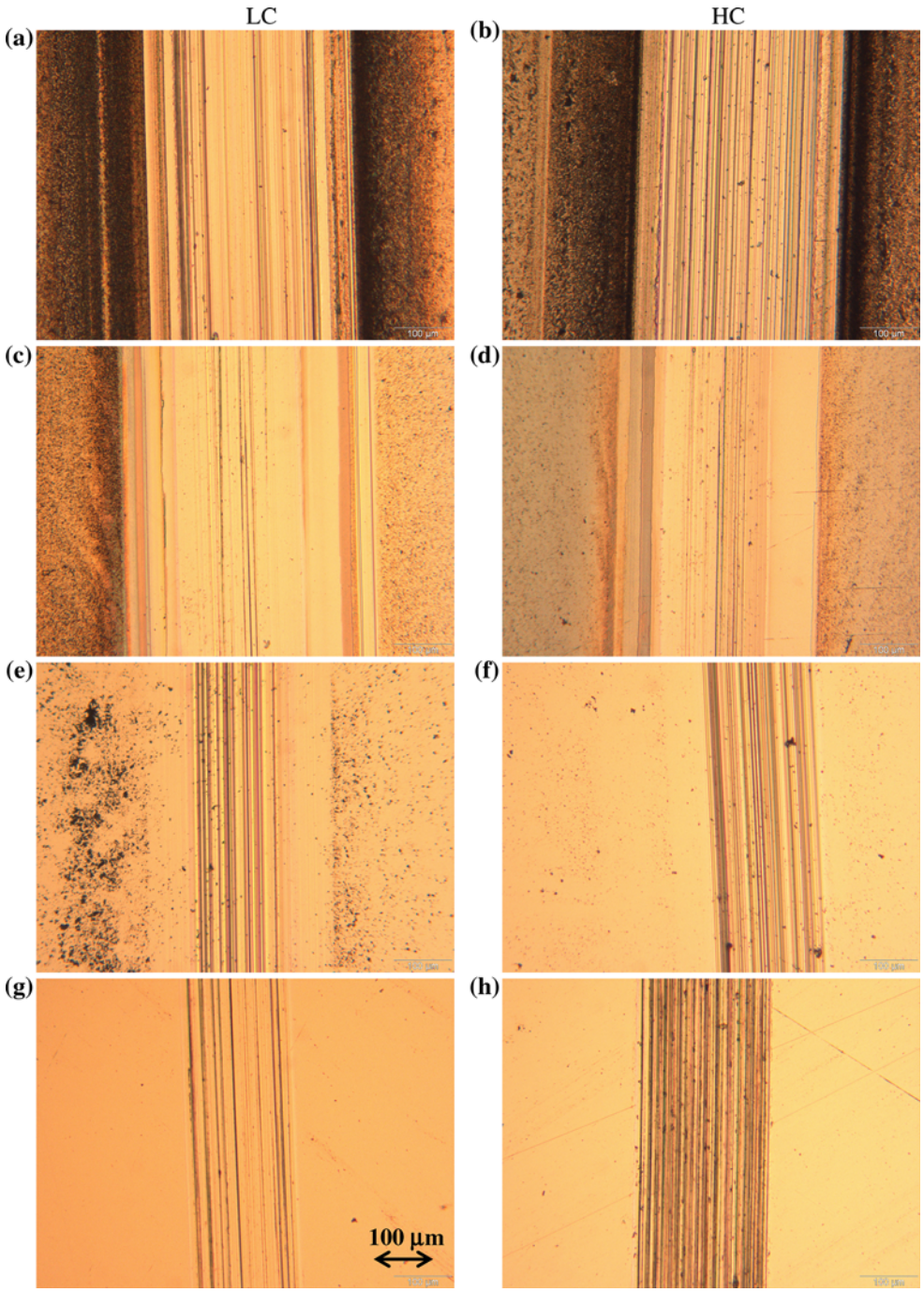


**Fig. 4** Optical microscopy images of wear trace LC and HC during sliding in **a**, **b** NaCl; **c**, **d** NaCl + albumin; **e**, **f** PBS and **g**, **h** PBS + albumin. Normal load is 1.2 N and applied potential −0.1 $V_{SCE}$. All images were taken with the same magnification

more complex behaviour than phosphate ions. It can act a cathodic inhibitor and it can promote the metal dissolution by complexing metallic ions [18] and by competing with phosphate in the adsorption on CoCrMo surfaces [18, 31]. The fact that albumin increases the corrosion currents indicates that the anodic catalyser effect is stronger than the cathodic inhibition. This effect is more pronounced in the PBS solutions because apparently the most relevant consequence of albumin presence is to limit the adsorption of the dissolution inhibiting phosphate ions.

The effect of alloy and adsorption processes can be also identified in the passive currents listed in Table 3. In NaCl solutions where adsorption effects are negligible the currents are higher for the HC alloy which metal matrix contains less chromium due to the precipitation of chromium carbides. Chromium is the main component of the

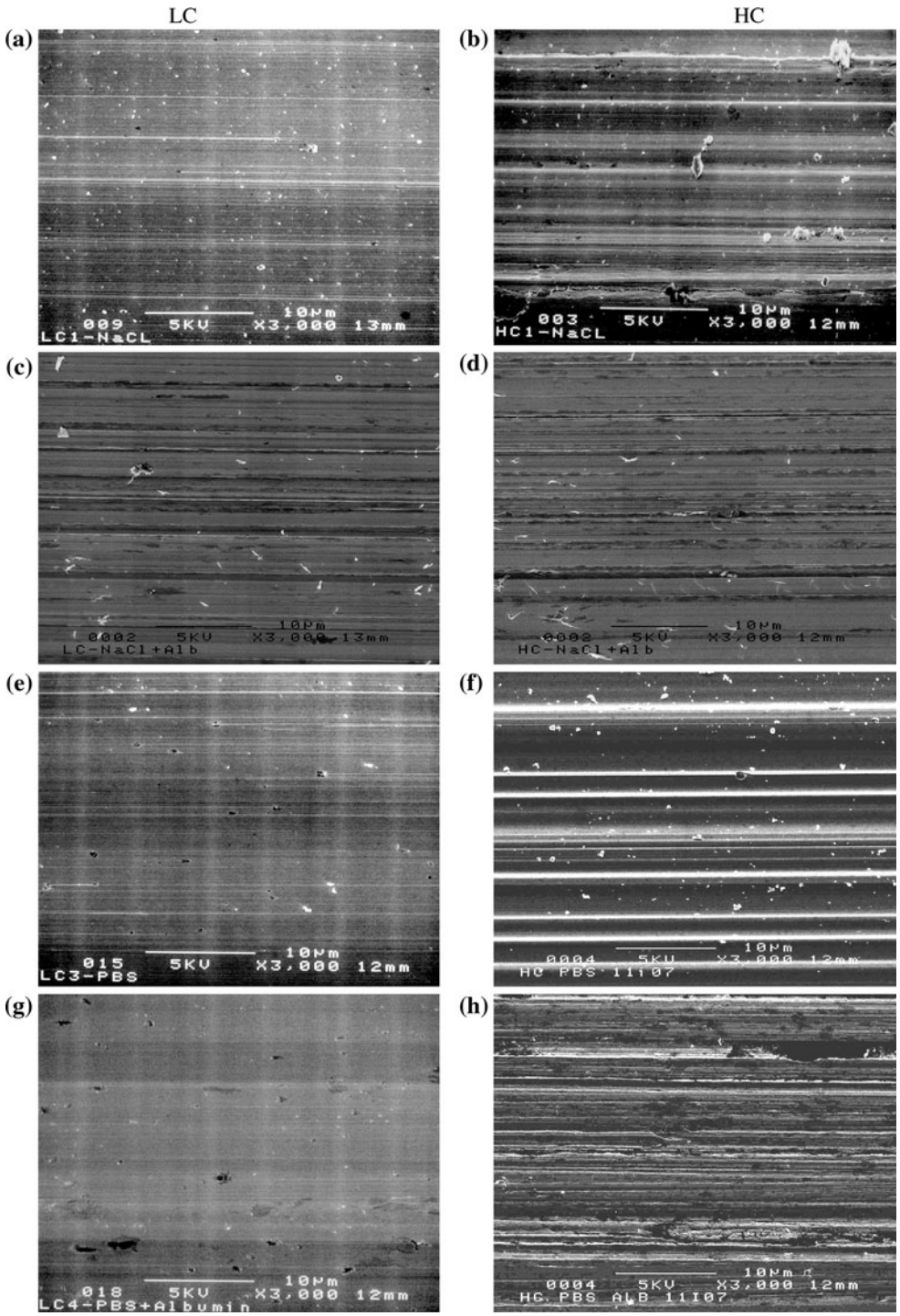


**Fig. 5** SEM images of wear tracks of LC and HC after sliding in **a**, **b** NaCl; **c**, **d** NaCl + albumin; **e**, **f** PBS and **g**, **h** PBS + albumin. Normal load is 1.2 N and applied potential −0.1 $V_{SCE}$

passive film [18, 31–33] and thus the LC alloy should exhibit a more protective film. In the PBS solution the adsorption of phosphate ions reinforce the passivity [31] of the alloys and accordingly lower passive current densities are found. The effect of albumin on the passive behaviour is much less pronounced than in the active state and in the PBS solution albumin slightly increases the passive current of both alloys. This behaviour was already observed in the corrosion current density values and was attributed to the competitive adsorption of phosphates and albumin [31].

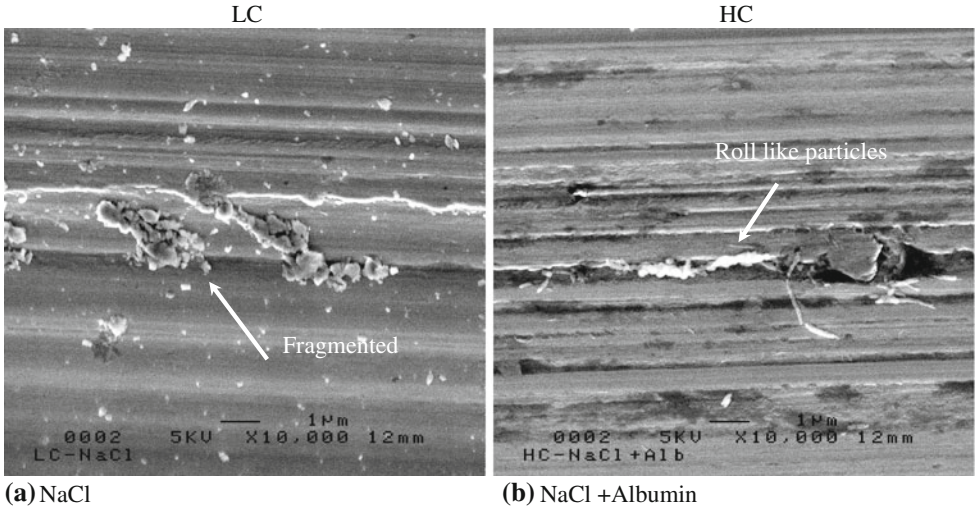


**Fig. 6** SEM detail images of wear debris formed at the end of the tribocorrision test of **a** LC in NaCl solution (after the friction transition) and **b** HC in NaCl + albumin solution (after the current transition). Normal load is 1.2 N and applied potential −0.1 $V_{SCE}$

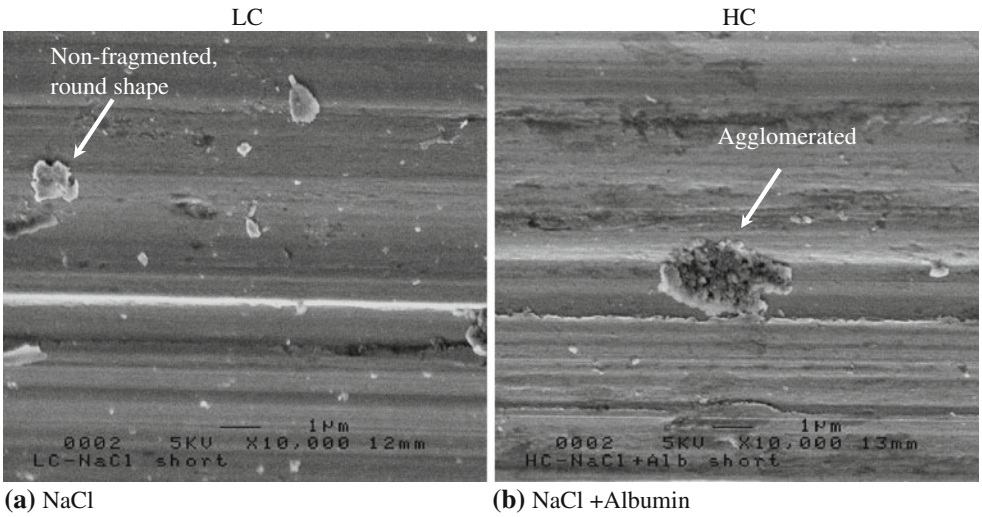


**Fig. 7** SEM detail images of wear debris formed during the tribocorrision test of **a** LC in NaCl solution (before the friction transition) and **b** HC in NaCl + albumin solution (before the current transition). Normal load is 1.2 N and applied potential −0.1 $V_{SCE}$

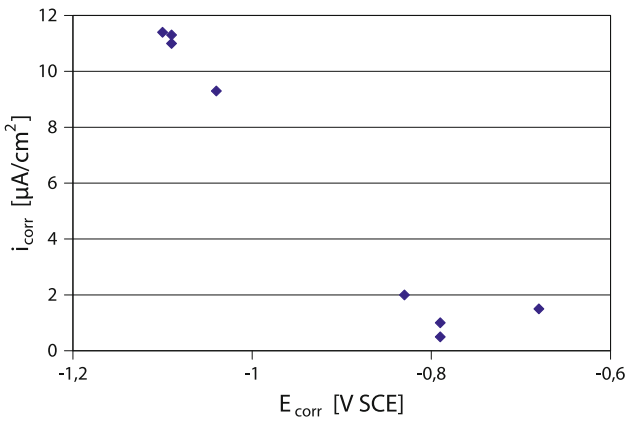


**Fig. 8** Corrosion potential versus corrosion current density of HC and LC alloys in simulated body fluids

### 4.2 Chemical and mechanical wear

In tribocorrosion it is common to distinguish two contributions to material removal: mechanical wear and wear accelerated corrosion [34]. The former mechanism corresponds to the release of metal particles by the abrasive action of the alumina ball. The latter mechanism results from removal of the passive film and the subsequent enhanced metal oxidation. The total wear corresponds to the sum of the mechanical wear volume $V_{mech}$ and the metal volume lost by wear accelerated corrosion $V_{chem}$ according to Eq. 1).

$$V_{tot} = V_{chem} + V_{mech} \quad (1)$$

The chemical volume $V_{chem}$ can be calculated from the wear track current $I_{sliding}$ (Table 4) using Faraday's law:

$$V_{chem} = \frac{I_{sliding} \cdot t \cdot M}{n \cdot F \cdot \rho} \quad (2)$$

where M is the atomic mass of the alloy, n is the charge number for the oxidation reaction (valence of oxidation was assumed 2.36 [33]), F is the Faraday constant (96500 C/mol), $\rho$ is the density of the alloy equal to 7.44 g/cm$^3$ and t is the duration of sliding, 3600 s.

The mechanical wear was calculated as difference between the wear volume and the chemical volume determined using Eq. 2.

Figure 9 allows one to compare the total wear volumes (Fig. 9a), the chemical (Fig. 9b) and mechanical (Fig. 9c) wear volumes as a function of solution and alloy type.

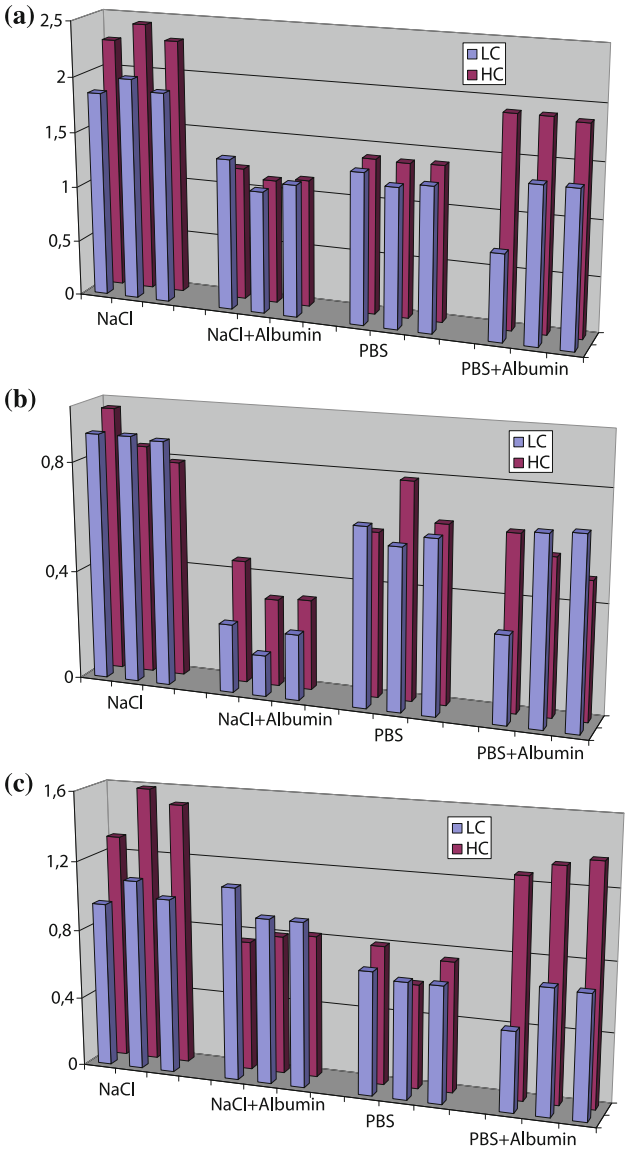


**Fig. 9** **a** Total wear volume, **b** chemical wear volume and **c** mechanical wear volume of LC and HC CoCrMo alloys in simulated body fluids. Normal load is 1.2 N and applied potential −0.1 $V_{SCE}$

From Fig. 9a it is evident that the wear ranking of the alloy depends significantly on the test electrolyte. The HC alloy wears more than the LC in the NaCl and in the PBS + albumin solutions while no significant differences are observed in the other electrolytes.

When differences appears between alloys this is mainly due to a difference in mechanical wear which is more pronounced in the HC alloy. This is likely related to the release of hard carbides that, as loose debris particles inside the contact, provoke abrasion as evidenced by the large abrasion scratches observed in the SEM images for the HC alloy only (Fig. 5b, f, h).

Friction does not seem to have a direct effect on mechanical wear. Indeed in the PBS + albumin solution the coefficient of friction is for both alloys approximately 0.4 while the mechanical wear varies by a factor of 2. In the PBS and in the NaCl + albumin solutions the same mechanical wear is observed although the coefficient of friction is 1 and 0.4, respectively.

The presence of scratches on nearly all the worn surfaces indicate that a three body abrasive situation is established within the contact through the presence of debris particles trapped within the alumina ball and the CoCrMo alloy sample. In this case mechanical wear depends on the abrasivity of the particles, the surface strength of the metal and the ejection probability of third body particles. By influencing surface chemistry, the composition of the solution can affect mechanical wear in different ways. First, passive films, which nature depends of electrolyte, may change the mechanical response of metals to sliding [35–38]. Further, oxidation, adsorption of ions or molecules can modify the repulsion/attraction forces between particles and solid surfaces and thus modify the local loading and wear [20, 39]. Inter-surface forces are expected to influence also the behaviour of carbide particles trapped in the contact and responsible for the scratching observed in Figs. 4 and 5. In the presence of albumin in NaCl small rolls like particle forms by agglomeration of smaller, adhering particles promoted by albumin. Indeed, Wood et al. [20, 40] reported that proteins promote the agglomeration of suspended ceramic particles used in micro-abrasion tests and thus reduces their abrasivity. The formation of this third body leads on the HC alloy to a smooth surface similar to the LC alloys. This suggests that in the NaCl–albumin solution the pulling out of carbides does not occur and abrasion is replaced by milder polishing wear. Clearly, the interpretation of wear mechanisms requires a fundamental understanding of the inter-surface mechanical interactions, their dependence on surface chemistry and their behaviour in tribological contacts. However this understanding is at present insufficient to explain in detail the effect of solution chemistry on the tribological response of the investigated alloys.

The type of alloy has little effect on chemical wear, which seems to be controlled by the nature of the solution. Only in the NaCl + albumin solution the HC alloys exhibits higher chemical wear as the current transition to lower values occurs later (Fig. 2). The quite similar behaviour in electrochemical response does not correlate with the large differences found in the polarisation curves, in particular in corrosion currents and in passive current densities between HC and LC. This is not surprising since the current during sliding is in principle governed by the extent of depassivation and by the passivation charge needed for film re-growth. Thus it depends on sliding kinematics, loading and passivation kinetics [41–43]. In pure electrochemical experiments the measured current corresponds to the sum of the contribution from anodic and cathodic reactions [29]. The current is limited by the charge transfer through the metal/electrolyte interface, which in turn depends on potential, surface structure, thickness and transport properties of the passive film.

### 4.3 Current and friction transitions

Similar transitions in currents as observed here in the NaCl + albumin solution were already reported by Yan et al. [17] during sliding of CoCrMo alloy in organic DMEM solutions and attributed to adsorption of organic molecules on the metal surface. In the present experiments current transitions are associated with the change in debris particles morphology from large to roll like particles (Figs. 7b, 6b, respectively). All these particles appear in the SEM images as conglomerates of smaller particles. Adsorbed albumin molecules can act as binder and thus provide the necessary cohesion to withstands the shear forces acting in the contact and to allow the formation of rolls [20]. As phosphates reduce adsorption of albumin they also limit particles cohesion and impedes the formation of rolls, as effectively observed in the present tests (Fig. 5).

Transitions in friction are also accompanied by changes in debris morphology as shown by Figs. 7a and 6a. However, a correlation between friction and particles morphology is not straightforward since friction is a complex phenomenon that may involve mechanical, chemical and physical responses from the metal and the counter piece. Indeed, the different debris morphologies as illustrated in Fig. 5b–d, g and h correspond all to the same coefficient of friction.

## 5 Conclusions

In this study the corrosion and tribocorrosion behaviour of a HC content CoCrMo alloy was compared to that of one LC CoCrMo alloy in four different simulated body fluids. Under the present experimental conditions the following conclusions could be drawn:

- The electrochemical behaviour in NaCl solution was specific to the alloy type and less sensitive to the presence or not of albumin. The PBS solution masked the alloy effect on the polarisation behaviour of the CoCrMo alloys that was largely affected by the presence of albumin. These effects were explained by the combined cathodic inhibiting and anodic catalysing action of albumin and its competitive adsorption with phosphates.
- The wear ranking of the HC and LC alloys is strongly dependent on the nature of the lubricating solution used. The HC alloy was found to wear more than the LC alloy in the NaCl and in the PBS + albumin solution while in the other solution wear was similar. This effect of solution chemistry could be related to enhancement of corrosion by sliding as well as to surface chemical effects affecting third body behaviour and mechanical wear.
- Observed transitions in friction and current were found to be associated to changes in debris morphology induced by the chemical composition of the solution.

As a general conclusion this study stresses out the crucial role played by chemical reactions between contacting material and environment and therefore the importance of considering surface chemical dependent phenomena in the evaluation of biomedical alloys.

**Acknowledgments** The authors thank J.-D. Neuvecelle for XRF analysis and P. Mettraux for the SEM analysis using the CIME-EPFL microscope. Plus Orthopaedics kindly provided the hip joint simulator heads.

## References

1. Rieker CB, Schön R, Köttig P. Development and validation of a second-generation metal-on-metal bearing: laboratory studies and analysis of retrievals. J Arthroplast. 2004;19:5–11.
2. Sargeant A, Goswami T. Hip implants: Paper V. Physiological effects. Mater Des. 2006;27:287–307.
3. Sargeant A, Goswami T. Hip implants: Paper VI. Ion concentrations. Mater Des. 2007;28:155–71.
4. Yan Y, Neville A, Dowson D, Williams S. Tribocorrosion in implants—assessing high carbon and low carbon Co-Cr-Mo alloys by in situ electrochemical measurements. Tribol Int. 2006;39:1509–17.
5. Wang A, Yue S, Bobyn JD, Chan FW, Medley JB. Surface characterization of metal-on-metal hip implants tested in a hip simulator. Wear. 1999;225–229:708–15.
6. Wang KK, Wang A, Gustavson LJ. Metal-on-metal wear testing of CoCr alloys. In: Disegi JA, Kenedy RL, Pilliar R, editors. Cobalt-base alloys for biomedical applications ASTM STP 1365. Conshohocken, PA: ASTM STP 1365; 1999. p. 135–44.
7. Tipper JL, Firkins PJ, Ingham E, Fischer J. Quantitative analysis of the wear and wear debris from low and high carbon content

cobalt chrome alloys used in metal on metal total hip replacements. J Mater Sci Mater Med. 1999;10:353–62.
8. St John KR, Poggie RA, Zardiackas LD, Afflitto M. Comparison of two cobalt-based alloys for use in metal-on-metal hip prostheses: evaluation of the wear properties in a simulator. In: Disegi JA, Kenedy RL, Pilliar R, editors. Cobalt-base alloys for biomedical applications ASTM STP 1365. West Conshohocken, PA: ASTM STP 1365; 1999. p. 145–55.
9. Scholes SC, Unsworth A. Pin-on-plate studies on the effect of rotation on the wear of metal-on-metal samples. J Mater Sci Mater Med. 2001;12:299–303.
10. Firkins PJ, Tipper JL, Ingham E, Stone MH, Farrar R, Fisher J. A novel low wearing differential hardness, ceramic-on-metal hip joint prosthesis. J Biomech. 2001;34:1291–8.
11. St John KR, Zardiackas LD, Poggie RA. Wear evaluation of cobalt-chromium alloy for use in a metal-on-metal hip prosthesis. J Biomed Mat Res. 2003;68B:1–14.
12. Cawley J, Metcalf JEP, Jones AH, Band TJ, Skupien DS. A tribological study of cobalt chromium molybdenum alloys used in metal-on-metal resurfacing hip arthoplasty. Wear. 2003;255: 999–1006.
13. Varano R, Bobyn JD, Medley JB, Yue S. Why is high carbon important in the tribology of metal-on-metal hip implants? In: 7th World Biomaterials Congress, 87; 2004.
14. Varano R, Bobyn JD, Medley JB, Yue S. Effect of microstructure on the dry sliding friction behaviour of CoCrMo alloys used in metal-on-metal hip implants. J Biomed Mat Res. 2006;76B: 281–6.
15. Varano R, Bobyn JD, Medley JB, Yue S. The effect of microstructure on the wear of cobalt-based alloys used in metal-on-metal hip implants. J Eng Med. 2006;220:145–59.
16. Chiba A, Kumagai K, Nomura N, Miyakawa S. Pin-on-disk wear behavior in a like-on-like configuration in a biological environment of high carbon cast and low carbon froged Co-29Cr-6Mo alloys. Acta Biomater. 2007;55:1309–18.
17. Yan Y, Neville A, Dowson D. Tribo-corrosion properties of cobalt-based medical implant alloys in simulated biological environments. Wear. 2007;263:1105–11.
18. Hiromoto S, Onodera E, Chiba A, Asami K, Hanawa T. Microstructure and corrosion behaviour in biological environments of the new forged low-Ni Co-Cr-Mo alloys. Biomaterials. 2005;26: 4912–23.
19. Wimmer MA, Loos J, Nassutt R, Heitkemper M, Fischer A. The acting wear mechanisms on metal-on-metal hip joint bearings: in vitro results. Wear. 2001;250:129–39.
20. Sun D, Wharton JA, Wood RJK. Micro-abrasion mechanisms of cast CoCrMo in simulated body fluids. Wear. 2009;267:1845–55.
21. Igual Muñoz A, Casaban Julian L. Influence of electrochemical potential on the tribocorrosion behaviour of high carbon CoCrMo biomedical alloy in simulated body fluids by electrochemical impedance spectroscopy. Electrochim Acta. 2010;55:5428–39.
22. Wood RJK, Sun D, Thakare MR, Frutos Rozas A, Wharton JA. Interpretation of electrochemical measurements made during micro-scale abrasion-corrosion. Tribol Int. 2010;43:1218–27.
23. Wimmer MA, Sprecher C, Hauert R, Täger G, Fischer A. Tribochemical reaction on metal-on-metal hip joint bearings—in vitro results. Wear. 2003;255:1007–14.
24. Stemp M, Mischler S, Landolt D. The effect of contact configuration on the tribocorrosion of stainless steel reciprocating sliding under potentiostatic control. Corros Sci. 2003;45:625–40.
25. Radice S, Mischler S. Effect of electrochemical and mechanical parameters on the lubrication behaviour of $Al_2O_3$ nanoparticles in aqueous suspensions. Wear. 2006;261:1032–41.
26. Landolt D, Mischler S, Stemp M. Electrochemical methods in tribocorrosion: a critical appraisal. Electrochim Acta. 2001;46: 3913–29.
27. Mischler S, Spiegel A, Stemp M, Landolt D. Influence of passivity on the tribocorrosion of carbon steel in aqueous solution. Wear. 2001;251:1295–307.
28. Igual-Muñoz A, Mischler S. Inter-laboratory study on electrochemical methods for the characterization of CoCrMo biomedical alloys in simulated body fluids (EFC 61). European Federation of Corrosion; 2010.
29. Landolt D. Corrosion and surface chemistry of metals. Lausanne: CRC Press; 2007.
30. Sims C. Cobalt based alloys. New York: Wiley; 1972. p. 260.
31. Igual-Muñoz A, Mischler S. Interactive effects of albumin and phosphate ions on the corrosion of CoCrMo implant alloy. J Electrochem Soc. 2007;154:C562–70.
32. Milosev I, Strehblow H-H. The composition of the surface passive film formed on CoCrMo alloy in simulated physiological solution. Electrochem Acta. 2003;48:2767–74.
33. Hodgson AWE, Kurz S, Virtanen S, Fervel V, Olsson COA, Mischler S. Passive and transpassive behaviour of CoCrMo in simulated biological solutions. Electrochim Acta. 2004;49: 2167–78.
34. Mischler S. Triboelectrochemical techniques and interpretation methods in tribocorrosion: a comparative evaluation. Tribol Int. 2008;41:573–83.
35. Favero M, Stadelmann P, Mischler S. Effect of the applied potential of the near surface microstructure of a 316L steel submitted to tribocorrosion in sulfuric acid. J Phys D Appl Phys. 2006;39:3175–83.
36. Bidiville A, Favero M, Stadelmann P, Mischler S. Effect of surface chemistry on the mechanical response of metals in sliding tribocorrosion systems. Wear. 2007;263:207–17.
37. Perret J, Boehm-Courjault E, Cantoni M, Mischler S, Beaudouin A, Chitty W, et al. EBSD, SEM and FIB characterisation of subsurface deformation during tribocorrosion of stainless steel in sulphuric acid. Wear (in press).
38. Espallargas N, Mischler S. Tribocorrosion behaviour of overlay welded Ni-Cr 625 alloy in sulphuric and nitric acids: electrochemical and chemical effects. Tribol Int. 2010;43:1209–17.
39. Kelsall GH, Zhu Y, Spikes HA. Electrochemical effects on friction between metal oxide surfaces in aqueous solutions. J Chem Soc Faraday Trans. 1993;89:267–72.
40. Sun D, Wharton JA, Wood RJK. Micro-abrasion-corrosion of cast CoCrMo—effects of micron and sub-micron sized abrasives. Wear. 2009;267:52–60.
41. Landolt D. Passivity issues in tribocorrosion. In: Philippe M, Vincent M, editors. Passivation of metals and semiconductors, and properties of thin oxide layers. Amsterdam: Elsevier Science; 2006. p. 477–87.
42. Mischler S, Spiegel A, Landolt D. The role of passive oxide films on the degradation of steel in tribocorrosion systems. Wear. 1999;225–229:1078–87.
43. Stemp M, Mischler S, Landolt D. The effect of mechanical and electrochemical parameters on the tribocorrosion rate of stainless steel in sulphuric acid. Wear. 2003;255:466–75.